Available online at www.sciencedirect.com
SCIENCE DIRECT
Journal of Power Sources 156 (2006) 400–413
JOURNAL OF POWER SOURCES
www.elsevier.com/locate/jpowsour

Computer experimental analysis of the CHP performance of a 100 kW_e SOFC Field Unit by a factorial design

M. Calì, M.G.L. Santarelli *, P. Leone

Dipartimento di Energetica, Politecnico di Torino, Corso Duca degli Abruzzi 24, 10129 Torino, Italy

Received 4 February 2004; received in revised form 26 May 2005; accepted 3 June 2005
Available online 8 September 2005

Abstract

Gas Turbine Technologies (GTT) and Politecnico di Torino, both located in Torino (Italy), have been involved in the design and installation of a SOFC laboratory in order to analyse the operation, in cogenerative configuration, of the CHP 100 kW_e SOFC Field Unit, built by Siemens-Westinghouse Power Corporation (SWPC), which is at present (May 2005) starting its operation and which will supply electric and thermal power to the GTT factory. In order to take the better advantage from the analysis of the on-site operation, and especially to correctly design the scheduled experimental tests on the system, we developed a mathematical model and run a simulated experimental campaign, applying a rigorous statistical approach to the analysis of the results.

The aim of this work is the computer experimental analysis, through a statistical methodology (2^k factorial experiments), of the CHP 100 performance. First, the mathematical model has been calibrated with the results acquired during the first CHP100 demonstration at EDB/ELSAM in Westerwoort. After, the simulated tests have been performed in the form of computer experimental session, and the measurement uncertainties have been simulated with perturbation imposed to the model independent variables. The statistical methodology used for the computer experimental analysis is the factorial design (Yates' Technique): using the ANOVA technique the effect of the main independent variables (air utilization factor U_{ox}, fuel utilization factor U_F, internal fuel and air preheating and anodic recycling flow rate) has been investigated in a rigorous manner. Analysis accounts for the effects of parameters on stack electric power, thermal recovered power, single cell voltage, cell operative temperature, consumed fuel flow and steam to carbon ratio. Each main effect and interaction effect of parameters is shown with particular attention on generated electric power and stack heat recovered.

Keywords: SOFC stack; CHP model; Computer experimental analysis; Factorial design

1. Introduction

The EOS Project – partners: Politecnico di Torino, Gas Turbine Technologies (GTT, Siemens group), Hysylab (Hydrogen System Laboratory) of Environment Park and Regione Piemonte – aim to create the main node of a regional fuel cell generator network. As a first step, the Pennsylvania-based Stationary Fuel Cells division of Siemens-Westinghouse Power Corporation (SWPC) supplied GTT with a CHP 100 kW_e SOFC Field Unit, fuelled by natural gas with internal reforming. The fuel cell is connected to the electricity national grid and provides part of the industrial district energy requirement. We referred to some papers to acquire some information before designing the cogeneration plant of the EOS-CHP 100 and we took advantage on this in planning the EOS-CHP 100 experimental campaign.

Most publications about SOFC mainly focus on single cell or involve aspects of the balance of plant (BoP) of a SOFC plant. These papers discuss fundamental scientific topics of the main cell elements and of the BoP devices: electrochemical reactions, fuel processing reactions, cell component overpotentials, materials and degradation of performances. Most papers describe the development of

* Corresponding author. Tel.: +39 011 564 4487; fax: +39 011 564 4499.
E-mail addresses: michele.cali@polito.it (M. Calì), massimo.santarelli@polito.it (M.G.L. Santarelli), pierluigi.leone@siemens.it (P. Leone).

0378-7753/$ – see front matter © 2005 Elsevier B.V. All rights reserved.
doi:10.1016/j.jpowsour.2005.06.033

Nomenclature

A	symbol of the factor U_{ox}
B	symbol of the factor U_F
C	symbol of the factor T_F
CHP	Cogeneration heat and power
D	symbol of the factor T_{ox}
E	symbol of the factor β
E_a	activation energy of anode (kJ mol^{-1})
E_c	activation energy of cathode (kJ mol^{-1})
E_{rev}	open circuit voltage (V)
f	f-value of the ANOVA analysis
F	Faraday number (C mol^{-1})
G	mass flow (kg s^{-1})
G_F	fuel mass flow (kg s^{-1})
h	specific enthalpy (kJ kg^{-1})
$\overline{h}$	molar enthalpy (kJ mol^{-1})
i	current density (A cm^{-2})
$i_{l,a/c}$	limiting current density at anode and cathode (A cm^{-2})
k	number of factors in the factorial analysis
K_a	pre-exponential coefficient for anode in activation overpotential (A m^{-2})
K_c	pre-exponential coefficient for cathode in activation overpotential (A m^{-2})
Kp	equilibrium constant of a chemical reaction
$Kp_{reforming}$	equilibrium constant of the reforming reaction
Kp_{shift}	equilibrium constant of the water shift reaction
m_a	anode activation overpotential exponential
m_c	cathode activation overpotential exponential
n	number of electrons involved in an electrode reaction
n_c	number of tubular cells in series in the stack
$n_{CH_4,inlet}$	number of methane moles at the inlet of the fuel mixer (mol s^{-1})
$n_{H_2O,rec}$	number of steam water moles recirculated from anode to fuel mixer (mol s^{-1})
n_i	total number of moles at fuel mixer inlet flow (mol s^{-1})
$n_{O_2,consumed}$	number of oxygen moles consumed inside the stack (mol s^{-1})
$n_{O_2,inlet}$	number of oxygen moles at the inlet of the stack (mol s^{-1})
$\dot{N}_k$	molar chemical reaction rate (mol s^{-1})
p	pressure (bar)
p_{stack}	stack operating pressure (bar)
R	universal gas constant (J mol^{-1} K^{-1})
R_a	resistance equivalent of the anode activation overpotential (Ω)
R_c	resistance equivalent of the cathode activation overpotential (Ω)
r	resistance of a layer in ohmic overpotential (Ω cm^2)
S	single cell active area (cm^2)
S/C	steam-to-carbon ratio
SOFC	solid oxide fuel cell
T	temperature (K)
T_F	fuel pre-heating temperature (°C)
T_{ox}	air pre-heating temperature (°C)
T_{stack}	stack operating temperature (°C)
t	thickness of a layer in ohmic overpotential (cm)
U_F	fuel utilization factor
U_{ox}	air utilization factor
V_c	single cell voltage (V)
w	effect of a factor evaluated through the Yates' Technique
W_{el}	stack electrical power (kW)
$W_{el,c}$	single cell electrical power (W)
x	moles of CH_4 which react (mol s^{-1})
y	moles of CO which react (mol s^{-1})
z	moles of H_2 which react (mol s^{-1})

Greek letters

ΔG	change in Gibbs free energy in a reaction (J mol^{-1})
Φ_{ech}	heat of electrochemical reaction (kW)
Φ_F	heat for fuel pre-heating (kW)
Φ_{ox}	heat for oxidant (air) pre-heating (kW)
Φ_{ref}	heat of steam reforming reaction (kW)
Φ_{shift}	heat of water shift reaction (kW)
Φ_{th}	stack recovered heat power (kW)
β	fraction of anode gas recycling
$\eta_{act,a/c}$	activation overpotential at anode and cathode (V)
$\eta_{conc,a/c}$	concentration overpotential at anode and cathode (V)
η_{ohm}	ohmic overpotential (V)
ρ_a	resistivity of anode layer (Ω cm)
ρ_c	resistivity of cathode layer (Ω cm)
ρ_{el}	resistivity of electrolyte layer (Ω cm)
ρ_{int}	resistivity of interconnection (Ω cm)

modeling studies of single solid oxide fuel cell or BoP, or the results of experimental analysis on single tubular or planar cell. Some other papers are devoted to the activity concerning SOFC power system's demonstrations.

In literature, many papers take into account a parametric analysis of a SOFC plant by changing the stack operating conditions. The aim of these approaches is to evaluate the performance of the plant by changing the BoP configuration internal or external fuel processing, combined heat and power generation plants or hybrid SOFC/GT plants [1–10]) or the generator operation and the fuel feeding. The effects of the modification of these variables were not analysed in depth with statistical methodologies, reducing to a qualitative

description of the effects on the performance of the simulated stack.

Some fundamental topics about SOFC are also presented by experimental characterization. Some papers point out the evaluation of the electrochemical behavior of SOFC anodes [11–16]. Other papers show experimental analysis in order to investigate degradation phenomena at cell's components under typical operating conditions; both macroscopic and micro-structural degradations are investigated like carbon deposition, delamination, nickel agglomeration, thermal cycling [16–29]; some studies focus on mechanical properties of SOFC materials by evaluating creeps or curvature under different test conditions [29–31].

1.1. Modeling approach

Modeling of SOFC generally involves two main approaches: the development of numerical tools with the aim to deeply describe chemical, electrochemical and thermal-fluid dynamics processes taking place in a single cell [32–42] or the development of zero-dimensional models with the aim of modeling a SOFC generator integrated in a more complex power generation plant. This approach allows to perform simulated generator steady-state operation with the possibility of taking suggestions about optimal BoP configuration or generator operation. In the development of our model, we referred mostly to the second approach. Some of the main considered papers are discussed.

In [1], the mathematical simulation of a planar solid oxide fuel cell (SOFC) is presented. It accounts for three-dimensional and time-dependent effects. Internal methane-steam reforming and recycling of the anode gas are also considered. In [2], a mathematical model of a tubular solid oxide fuel cell (SOFC) is presented. The complete electrochemical and thermal factors are accounted for in a rigorous manner. Comparison is made with single cell test data from Westinghouse. In [3], the aim of the work is to investigate of internal reforming solid oxide fuel cell and gas turbine combined cycles. A mathematical model has been developed that simulates fuel cell steady-state operation, the model has been used for a complete parametric analysis; after in [4] both an exergy and a thermoeconomic analysis of the proposed cycles have been carried out; recently in [5] presented a work dealing with the design and off-design performance evaluation of an anodic recirculation system based on ejector technology for solid oxide fuel cell hybrid applications. In [6], a thermodynamic model of a tubular SOFC stack is proposed. It is then calibrated on the available data for a recently demonstrated tubular SOFC prototype plant (Westerwoort; CHP 100 Siemens). In [7], a detailed BoP has been investigated. An energy and economic analysis of a decentralized natural gas-fuelled SOFC-power plant in the range of 200 kW capacity is carried out. All the calculations start from a basic plant concept with a simple flowsheet and a basic parameter set of SOFC operation and economic data. Changes in costs of electricity and plant efficiency are determined for the variation of the cell operation parameters. This includes the influence of the air temperature increase in the stack, degree of internal reforming, cell voltage and fuel utilization; in the Part II of the paper [8], the flowsheet of the SOFC BoP is changed considering gas recycling by blowers or jet boosters.

Some articles presented recently SOFC technology demonstrations and SOFC state of the art and future perspectives [43–48]. In particular, in [43] the Siemens's Field Unit demonstration program including the first SOFC CHP 100 demonstration at EDB/ELSAM in Westerwoort (Holland), the Southern California Edison SCE 220-kW and pressurized SOFC/gas turbine (PSOFC/GT) power system are described.

1.2. Aims of the paper

Some authors finalized their papers in a parametric analysis of a SOFC system. In [3,4,6–8], the effects of cell temperature, cell pressure, recirculation ratio of anode exhaust, utilization ratios of fuel and air, and average current density on both the electric and thermal performances of a solid oxide fuel cell were calculated under typical operating conditions. The effects of these operation independent variables were not analysed in depth with statistical methodologies, reducing to a description of a parametric analysis.

Now, we are planning the experimental campaign of the EOS Project and, in order to take the better advantage from the analysis of the on-site operation, and especially to correctly design the scheduled experimental tests on the system, we developed a model of the EOS-CHP 100 and run a simulated experimental campaign, applying a rigorous statistical approach to the analysis of the results.

The aim of our paper is therefore the experimental analysis, through a statistical methodology, of the single and combined effects of the main stack operation independent variables on the cogenerative (electricity and heat) performance of a tubular SOFC stack integrated system.

The tests have been performed in the form of a computer experimental session, based on a simulation model of the stack. The measurement uncertainties are simulated with perturbation imposed to some independent variables.

The statistical methodology used for the computer experimental data analysis has been the factorial design (Yates' Technique): using analysis of variance (ANOVA) we have analysed the significance of the main operation independent variables (factors: air utilization factor, fuel utilization factor, fuel pre-heating temperature, air pre-heating temperature, fraction of anode gas recycling) considering their single and combined effects on the electric and thermal power which could be recovered from the stack system.

2. Description of SOFC stack and BoP

The EOS-CHP 100 Field Unit is the first field unit to utilize the commercial prototype of air electrode supported cell and

Fig. 1. Picture of the EOS-CHP 100 SOFC Field Unit installed at the GTT factory.

in-stack reformers (Fig. 1). In the design used in the EOS-CHP 100 SOFC Field Unit, the cell components are deposited in the form of thin layers on the air electrode (cathode) tube (air electrode-support AES) closed at one end. The size of the complete tube is 150 cm length and 2.2 cm diameter with an external surface (anode side) of 834 cm^2 [43–47]. The next level of fabrication hierarchy after the cell is the cell bundle, which consists of a 24-cell array arranged as eight cells in electrical series by three cells in electrical parallel. Four cell bundles are connected in series to form a bundle row, and 12 bundle rows are aligned side by side, interconnected in serpentine fashion with an in-stack reformer between each bundle row (4 bundles in 12 rows, for a total of 1152 single tubes). An advantage of all cathode-supported single cells is a three-dimensional penetration structure in-between cathode and electrolyte that is achieved during electrolyte deposition. This leads to a decrease of cathodic polarization losses [45].

A detailed description of materials and geometry characterizing a single solid oxide fuel cell tube could be found in literature [43–47].

Considering the total volume of the EOS-CHP 100 SOFC Field Unit, just the 25% is occupied by the stack. The rest of the system is composed by the *balance of plant* (BOP), including five major skids: Generator Module, Electrical Control System, Fuel Supply System (FSS), Thermal Management System (TMS) and Heat Export System (HES). The simplified flow schematic of the BOP of the EOS-CHP 100 SOFC Field Unit is shown in Fig. 2.

The stack is integrated with a catalytic pre-reformer for the natural gas-fuel, and a combustor where the post-combustion of the depleted fuel and air exiting the cell occurs. Before entering the stack, the fuel flow is desulfurized and then sent to the ejectors in the stack. Part of the anode exhaust gases is recirculated in the fuel stream (to supply water for the fuel internal reforming reaction). Since the generator operates at high temperature (around 970 °C), a heat flow from the stack exhausts can be recovered at the outlet of the plant. Considering the assessment of the BoP of the EOS-CHP 100, the exhausts leave the generator skid at around 850–900 °C. After, in the thermal management system (TMS) they exchange energy with the incoming process air (in the low temperature recuperator (LTR) and in the high temperature recuperator (HTR)); at the TMS outlet, at nominal operating condition (generator current 500 A and $U_F = 0.85$)

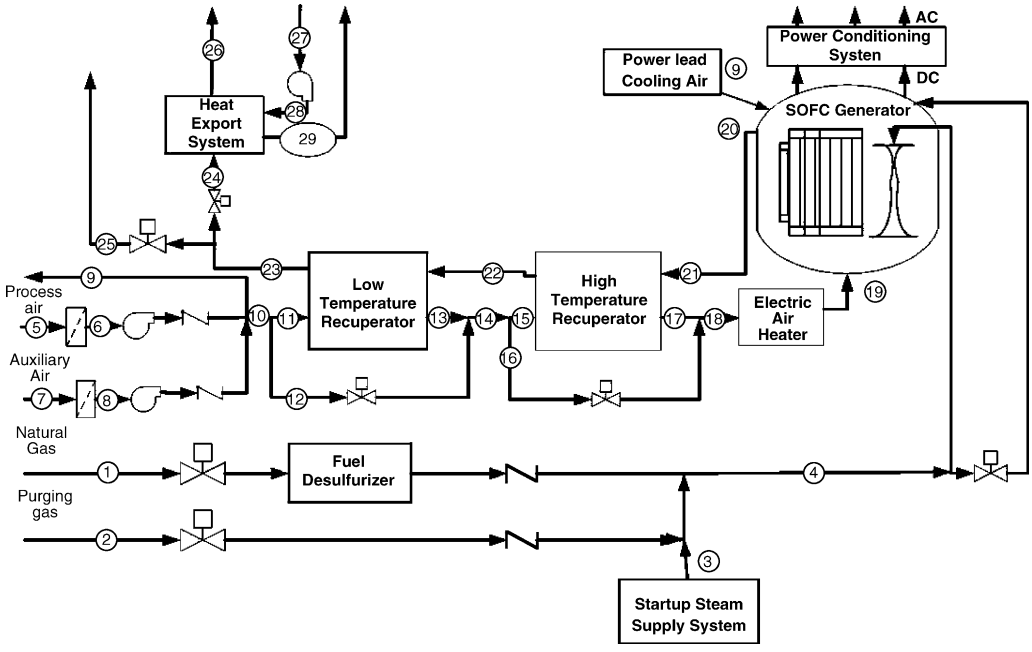

Fig. 2. Simplified flow schematic of the balance of plant of the EOS-CHP 100 SOFC Field Unit.

the exhausts temperature is around 250 °C. In the heat export system, the heat is recovered from the stack exhausts in order to heat a pressurized water flow which will be used in the heating system of the GTT factory (during Winter) or to produce cooling power in an absorption chiller (during Summer). Therefore, the present configuration of the EOS-CHP plant is a trigeneration energy system. The auxiliaries are: process air blowers, air filters, purging gas vessels, start-up and control systems [43–45].

In the nominal operation point ($I = 500$ A, corresponding to 0.2 A cm^{-2}), the DC electric efficiency is 53.25%, while the AC electric efficiency is 46%, while the cogenerative efficiency (AC electric + recovered thermal energy) is in the order of 74–75%.

3. SOFC stack model

Modeling the SOFC stack involves the electrochemical and chemical models. The electrochemical model refers to the polarization curve. The chemical model considers the reactions taking place in the stack: fuel processing reactions (steam reforming, water shift).

The subsequent balance of plant will integrate the stack model with a thermal model (taking into account the energy balance equations) and a chemical species mass balance for the balance of plant.

3.1. Electrochemical model

The polarization curve for a solid oxide fuel cell is expressed by the Eq. (1):

$$V_c = E_{rev} - \eta_{act,a/c} - \eta_{ohm} - \eta_{conc,a/c} \quad (1)$$

where V_c is the single cell voltage, E_{rev} the open circuit voltage, $\eta_{act,a/c}$ the activation overpotential, η_{ohm} the ohmic overpotential and $\eta_{conc,a/c}$ is the concentration overpotential.

Most of the considered equations are suggested by current literature, and they are shown in Table 1. In particular, the equations modeling the resistivities have a good agreement with the available experimental data in the range of current density up to 0.3 A cm^{-2}; after this value, the models are less performing. Up to now, the available data describing the real operation of the stack never reached values higher than 0.3 A cm^{-2}.

3.2. Chemical model

The chemical model accounts for internal fuel processing (steam reforming, water shift) reactions:

$$\text{Steam reforming}: \quad CH_4 + H_2O \leftrightarrow 3H_2 + CO \quad (10)$$

$$\text{Water shift}: \quad CO + H_2O \leftrightarrow H_2 + CO_2 \quad (11)$$

Table 1
Equations of the electrochemical model

Activation overpotential $\eta_{act,a/c}$ [1]
(2)Cathode $\frac{1}{R_c} = K_c \cdot \frac{4F}{RT} \cdot \left(\frac{p_{O_2}}{p^0}\right)^{m_c} \exp\left(-\frac{E_c}{RT}\right)$
(3)Anode $\frac{1}{R_a} = K_a \cdot \frac{2F}{RT} \cdot \left(\frac{p_{H_2}}{p^0}\right)^{m_a} \exp\left(-\frac{E_a}{RT}\right)$

Ohmic overpotential η_{ohm} [2,32]
(4)$\eta_{ohm} = i\sum_j r_j; \quad r_j = \rho_j t_j$
(5)Anode $\rho_a = 0.008114 \exp\left(\frac{600}{T}\right)$
(6)Electrolyte $\rho_{el} = 0.00294 \exp\left(\frac{10350}{T}\right)$
(7)Cathode $\rho_c = 0.00298 \exp\left(\frac{-1392}{T}\right)$
(8)Interconnection $\rho_{int} = 0.1256 \exp\left(\frac{4690}{T}\right)$

Concentration overpotential $\eta_{conc,a/c}$
(9)Anode/cathode $\eta_{conc,a/c} = \frac{RT}{nF} \ln\left(1 - \frac{i}{i_{l,a/c}}\right)$

Constants
Activation energy of anode 110 kJ mol^{-1}
Activation energy of cathode 160 kJ mol^{-1}
Pre-exponential coefficient for anode $K_a = 2.13 \times 10^8$ A m^{-2}
Pre-exponential coefficient for cathode $K_c = 1.49 \times 10^{10}$ A m^{-2}
Anode activation overpotential exponential $m_a = 0.25$
Cathode activation overpotential exponential $m_c = 0.25$

These reactions are considered at equilibrium. For both reactions, the equilibrium constant is calculated as:

$$\ln K_p(T) = \frac{-\Delta G(T, p^0)}{RT} \quad (12)$$

Eq. (12) can be used integrated by a correlation linking directly to the temperature at which reaction takes place:

$$\log K_p(T) = AT^4 + BT^3 + CT^2 + DT + E \quad (13)$$

The parameters A–E of the JANAF tables have been found in literature [3].

4. BoP model

The BOP model accounts for devices, which define the SOFC's plant. These components are: blowers, desulfurizers, purging gas tanks, pre-reforming reactor, reformer, heat exchangers used to pre-heat inlet gases (fuel gas, air), heat exchanger to export heat by wasted stack gases (HES, heat export system) and post-combustion chamber.

The hypothesis for the BoP model are:

- steady-state condition;
- zero-dimentional aproach;
- cathodic flow composition: mixed flow of N_2 and O_2;
- anodic flow composition: mixed flow of CH_4, CO_2, CO, H_2, H_2O, N_2;
- internal fuel processing: reforming and CO-shift reactions at equilibrium;

Table 2
Equations of the BoP model

Mixer mass balance $G_6 = G_3 + G_5$ (15)
Mixer thermal balance $G_6 h_6 = G_3 h_3 + G_5 h_5$ (16)
Steam to carbon ratio (S/C) $\mathrm{S/C} = \frac{n_{\mathrm{H_2O,rec}}}{n_{\mathrm{CH_4,inlet}}}$ (17)
Oxidant consumption $n_{\mathrm{O_{2inlet}}} = n_{\mathrm{O_{2consumed}}}/U_{\mathrm{ox}}$ (18)
Heat of steam reforming reaction $\phi_{\mathrm{ref}} = x \cdot (3\overline{h}_{\mathrm{H_2}} + \overline{h}_{\mathrm{CO}} - \overline{h}_{\mathrm{H_2O}} - \overline{h}_{\mathrm{CH_4}})$ (19)
Heat of water shift reaction $\phi_{\mathrm{shift}} = y \cdot (\overline{h}_{\mathrm{H_2}} + \overline{h}_{\mathrm{CO_2}} - \overline{h}_{\mathrm{CO}} - \overline{h}_{\mathrm{H_2O}})$ (20)
Heat of electrochemical reaction : $\phi_{\mathrm{ech}} = n_{\mathrm{c}} \cdot I \cdot \left(\frac{-\Delta\overline{h}(T_{\mathrm{stack}})}{2F} - V_{\mathrm{c}}\right)$ (21)
Cell electrical power : $W_{\mathrm{el,c}} = i_{\mathrm{c}} S V_{\mathrm{c}}$ (22)
Fuel pre-heating : $\phi_{\mathrm{F}} = G_{\mathrm{F}} \cdot (h_1 - h_3)$ (23)
Oxidant pre-heating : $\phi_{\mathrm{ox}} = G_{\mathrm{ox}} \cdot (h_2 - h_4)$ (24)
Heat recovered : $\phi_{\mathrm{th}} = \lvert h_8 - h_7 \rvert$ (25)
BoP thermal balance : $W_{\mathrm{el}} = h_1 + h_2 - h_8 - \phi_{\mathrm{th}} - \phi_{\mathrm{d\_1}} - \phi_{\mathrm{d\_2}} - \phi_{\mathrm{d\_shell}} + \sum_K \dot{N}_k(-\Delta H)$ (26)

- model does not account for direct oxidation of CO at cell anode;
- gas temperatures at outlet conditions from the reformer and the stack are, respectively, reforming temperature and operating cell temperature;
- internal water and thermal management.

The model solves a non-linear system of equations. The composition of the anodic recycling gas is then calculated:

$$\begin{cases} \mathrm{Kp_{reforming}} = \dfrac{\left(\dfrac{\mathrm{CO}_i + x - y}{n_i + 2x}\right) \cdot \left(\dfrac{\mathrm{H_2}_i + 3x + y - z}{n_i + 2x}\right)^3}{\left(\dfrac{\mathrm{CH_4}_i - x}{n_i + 2x}\right) \cdot \left(\dfrac{\mathrm{H_2O}_i - x - y + z}{n_i + 2x}\right)} p_{\mathrm{stack}}^2 \\ \mathrm{Kp_{shift}} = \dfrac{\left(\dfrac{\mathrm{H_2}_i + 3x + y - z}{n_i + 2x}\right) \cdot \left(\dfrac{\mathrm{CO_2}_i + y}{n_i + 2x}\right)}{\left(\dfrac{\mathrm{CO}_i + x - y}{n_i + 2x}\right) \cdot \left(\dfrac{\mathrm{H_2O}_i - x - y + z}{n_i + 2x}\right)} \\ z = U_{\mathrm{f}} \cdot (3x + y + \mathrm{H_2}) \end{cases} \quad (14)$$

Evaluated x, y and z it is possible to define the anode exhaust composition. Most of the considered equations are listed in Table 2.

All the described chemical and electric calculations need the knowledge of the stack temperature. A tentative stack temperature is assumed and the cell characteristics evaluated. Then, the enthalpy variation inside the stack is calculated and a new stack temperature obtained. The process is iterated until the satisfaction of a prescribed tolerance.

The results obtained with the model have been compared with the experimental data of the CHP 100 acquired during its first installation at EDB/ELSAM (Westervoort), data which we have used for the first validation of the model.

5. Methodology and computer experimental design

Several variables can be used to characterize the stack operation, and they can be considered as dependent variables. These dependent variables of the stack are influenced by several other independent variables (in the following defined *factors*), and to analyse their influence an experimental design methodology is fundamental. In this work, the experimental tests have been performed in the form of a computer experimental session, based on the simulation model of the stack; the measurement uncertainties are simulated with perturbation imposed to the independent variables. Therefore, a full factorial design of experiments has been employed: an output (dependent) variable could be correlated to the input (independent) variables (or factors) pointing out its effect. So, it is possible to find which factors deserve a particular attention: for example, in the case of a significant factor a further analysis could be done or more accuracy could be necessary; on the contrary, the factors having a negligible effect could even be not considered in subsequent analysis. Also, the combined effects among the factors can be assessed.

Once the k input factors have been chosen, it is fundamental to determine their range of variation (the experimental domain). If the experiments are performed only at the extreme of the range of variation of the factor (that is, only two levels of the factor are considered), 2^k experiments are required, and each different combination of different factor levels is called treatment. If the treatment is replicated then an analysis of variance can be performed.

Concerning the adopted symbolism, each factor is labelled with a capital letter; to describe the treatments, a lowercase letter is used when the factor is at the upper level, while the letter is omitted when it is at its lower level; when all the factors are at the lower level, the notation (L) is used. To analyse the effects of the main factors the well-known Yates' Technique has been employed: the treatment combinations must be therefore written down in standard form [48,49]. The effects of the factors (indicated with the letter w), are distinguished in main effects ($\mathrm{w_A}$, $\mathrm{w_B}$, ...), and interaction effects ($\mathrm{w_{AB}}$, $\mathrm{w_{AC}}$, ...).

In the experiment session discussed in the paper, five factors have been chosen, with three test replications. Therefore, a total of $2^5 \times 3 \times 2 = 192$ computer experiments have been necessary to obtain all the possible effects and interactions. The five factors chosen have been: air utilization factor U_{ox}, fuel utilization factor U_{F}, fuel pre-heating temperature T_{F}, air pre-heating temperature T_{ox}, fraction of anode gas recycling β.

The range of the factors is shown in Table 3.

In order to apply the Yates' method and to evaluate the main and the interaction effects of the factors, we need repetitions on the experiments. Therefore, randomized

Table 3
Factors analysed (each factor is labelled with a capital letter) and their levels

Factor	Description	Lower level (−)	Upper level (+)
A	U_{ox}	0.2	0.3
B	U_{F}	0.7	0.9
C	T_{F} (°C)	200	400
D	T_{ox} (°C)	700	850
E	β	0.6	0.7

Table 4
Randomized uncertainties used to modify the factor values

Factor	Uncertainty
U_{ox} (%)	5
U_F (%)	2
T_F (°C)	±1
T_{ox} (°C)	±1
β (%)	5

uncertainties on the selected factors (representing independent variables of the model, and set points for the real operation) and on the current (independent variable of the model, and set point for the real operation) have been introduced. The aim was to simulate a real experimental measurement, and the randomized uncertainties take into account the errors of a real instrument. The evaluated effects are related to the significance of a factor macroscopic variation on some dependent variables, and not to the effect of a factor measurement error on the dependent variables. The randomized uncertainties used to modify the factors values are shown in Table 4.

Six outputs are investigated in this work: the electric W_{el} and recovered heat power Φ_{th} outputs; the fuel mass flow G_F; the single cell voltage V_c; the stack temperature T_{stack}; the steam-to-carbon ratio S/C.

To reduce the number of experiments, only two operating conditions have been analysed at two different current density values (0.2 and 0.4 A cm^{-2}), introducing also a randomized uncertainty on the current data (1%, simulating the uncertainty in the current acquisition). The factorial analysis was done at the indicated two current densities, for every dependent variable. These values of current density have been chosen because higher values are not realistic for the analysed stack. Actually, even the value of 0.4 A cm^{-2} is very high, but some reports states that it could be reached at operating temperatures higher than 900 °C with a cell voltage around 0.47 V [43].

The computer experimental campaign has been carried out considering the EOS-CHP100 fed with dry methane.

6. Results and discussion

6.1. Electric power

6.1.1. Considerations about main and interaction effects

The main and interaction effects on electric power are shown in Fig. 3 (low current density) and Fig. 4 (high current density).

Factors with no significant effects: An interesting notation is that the fuel preheating temperature has no effect on the electric power produced; therefore, the fuel preheating could be avoided. Moreover, even the anode gas recycling fraction shows no significant effects, and therefore it could be fixed at the value indicated by the plant manuals.

U_{ox} at high level: Positive main effect, because of better performances in terms of internal thermal management and single cell electric efficiency, due to increase of cell temperature and decrease of cell overpotentials.

U_F at high level: Negative main effect, due to decrease of hydrogen partial pressure at cell anode, decrease in Nernst voltage.

T_{ox} at high level: Positive main effect, due to increase of cell temperature and decrease of cell overpotentials.

U_F at high level, T_{ox} at high level: Negative effect, because of prevailing negative effect of U_F at high level.

U_F at high level, β at high level: Treatment combinations with high fuel utilization and high anode gas recycling fraction have a minor negative effect, because of the negative effect of U_F at high level and of the excess water in case of higher fraction of anode gas recycling.

Main and interaction effects at high cell current: At high cell currents the main effects of the factors are increased because of bigger mass flows inside the stack; moreover, at high cell current the fraction of anode gas recycling has a main minor negative effect on electric power, because of the excess water concentration at the anode side amplified at high current.

6.1.2. Analysis of the effects of the significant factors

The effect of the air utilization factor is shown in Fig. 5.

The curves with high air utilization factor show higher values of stack electric power at various current density values. A higher U_{ox} means a lower air mass flow, and therefore a higher stack equilibrium temperature (at fixed conditions). The higher stack temperature causes an increase of the cell voltage: it is possible to obtain especially a reduction of the activation and ohmic overvoltages.

The effects are increased at high current densities, because the air mass flows are greater and this amplifies the effects of changing the air utilization factor.

A factor causing significant effects on the stack electric power is the air pre-heating temperature T_{ox}, as shown in Fig. 6.

The increase of the air pre-heating temperature causes an increase of the stack equilibrium temperature, and consequently an increase of the cell voltage: it is possible to obtain especially a reduction of the activation and ohmic overvoltages. The effects are increased at high current densities, because the air mass flows are greater and this amplifies the effects of changing the air utilization factor.

Another factor causing significant effects on the stack electric power is the fuel utilization factor U_F, as shown in Fig. 7.

An increase of the factor U_F determines a reduction of the stack electric power; this is due to a reduction of the cell voltage, caused by an increase of the molar fraction of H_2O in the anode mixture, with a consequent reduction of the molar fraction of H_2 on the electrode surface, as shown in Table 5.

As usual, the effects are emphasized at higher currents due to the higher mass flows.

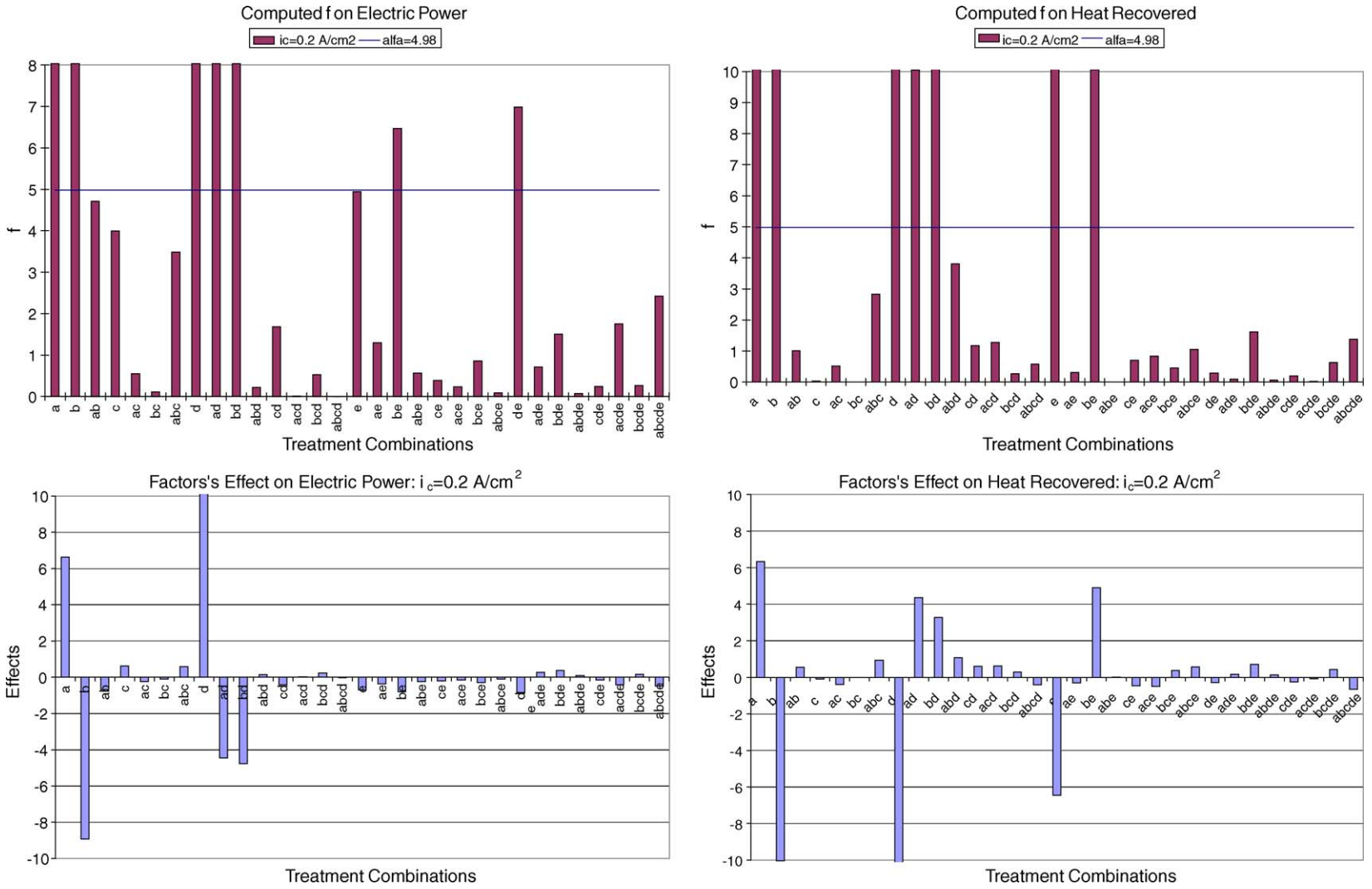

Fig. 3. Computed *f*-value and effects of the parameters on stack electric power and heat recovered at $i = 0.2\ \mathrm{A\,cm^{-2}}$.

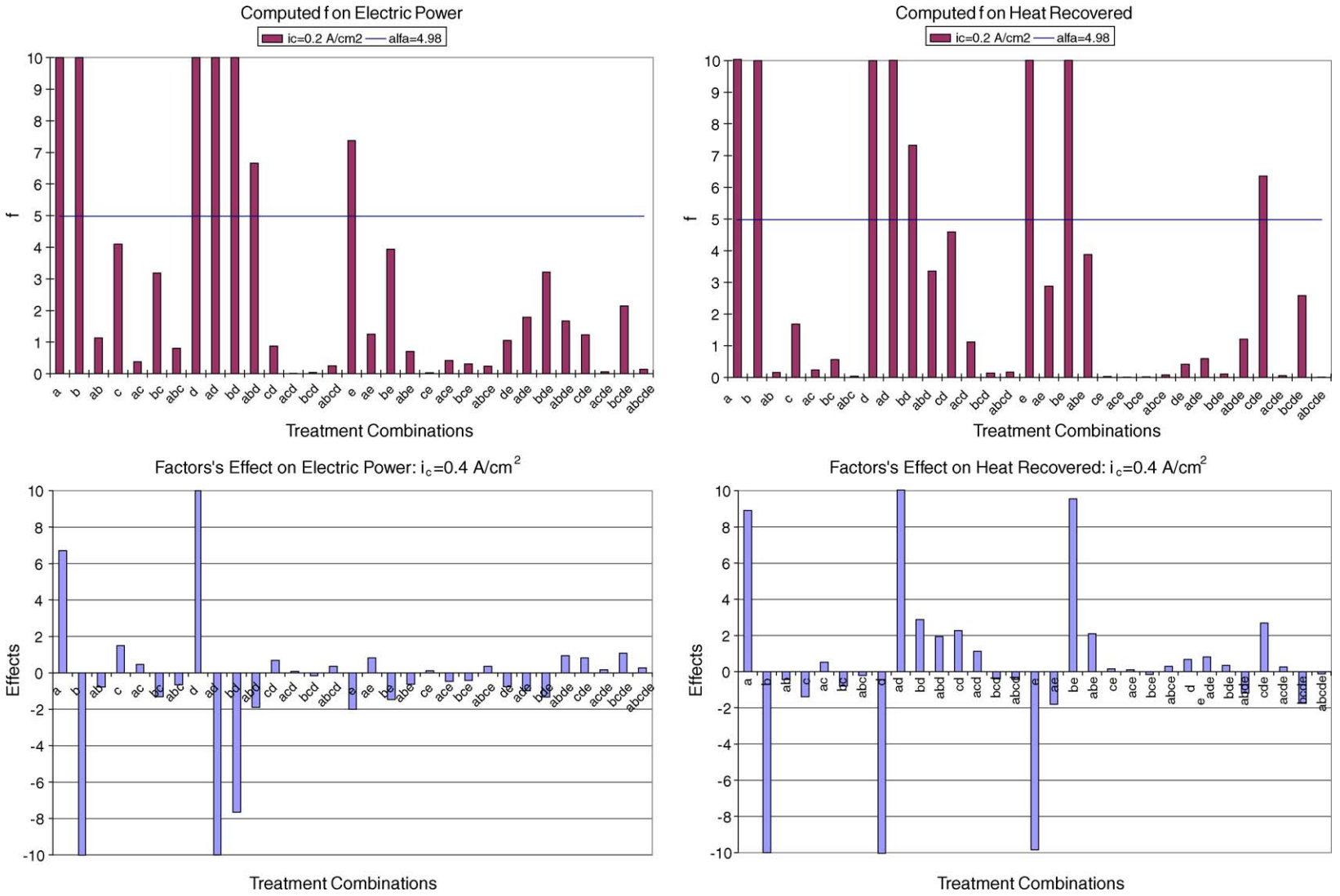

Fig. 4. Computed f-value and effects of the parameters on stack electric power and heat recovered at $i = 0.4\ \mathrm{A\,cm^{-2}}$.

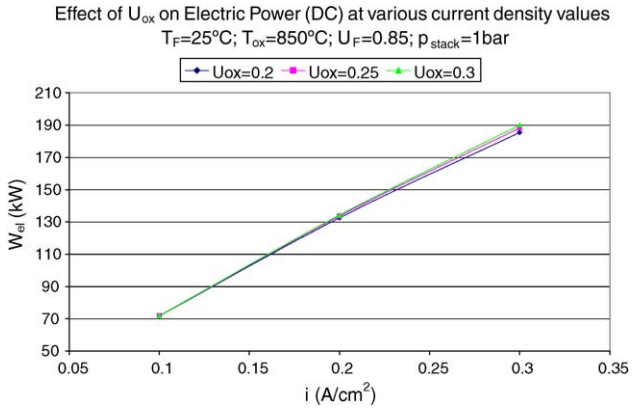

Fig. 5. Effect of the air utilization factor on stack electric power.

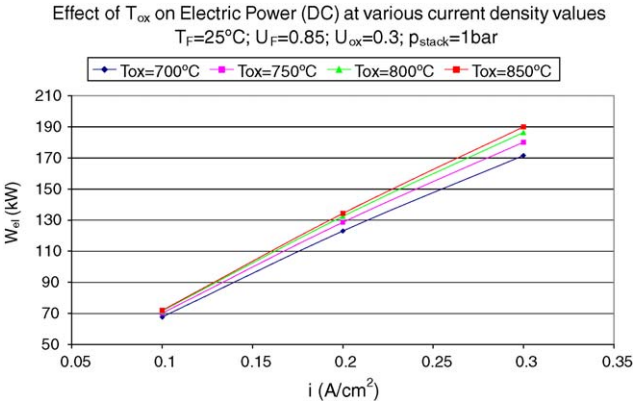

Fig. 6. Effect of the air pre-heating temperature on stack electric power.

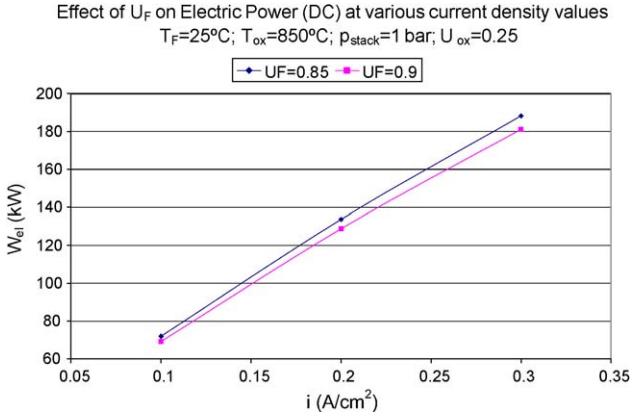

Fig. 7. Effect of the fuel utilization factor on stack electric power.

Table 5
Effect of U_F on the molar fraction of H_2 on the anode mixture and consequent effect on the cell open circuit voltage

Treatment combination	y_{H_2O}	y_{H_2}	y_{CO}	y_{CO_2}	E_{rev}
(*L*)	0.4858	0.148	0.06	0.3062	0.864
b	0.6114	0.0452	0.025	0.3184	0.777

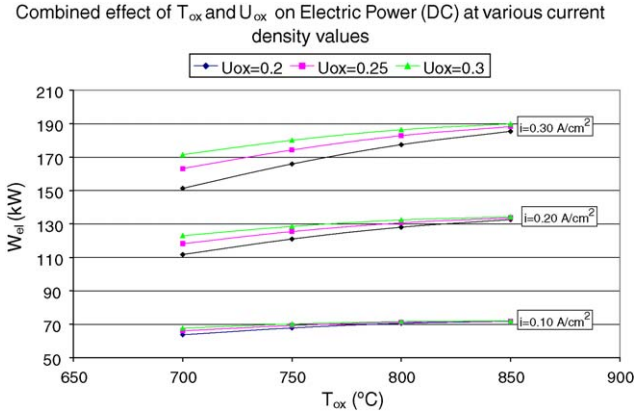

Fig. 8. Combined effect of the air utilization factor and the air pre-heating temperature on stack electric power.

It is interesting to analyze the effects of some factor combinations. The factor combinations with a significant effect on the stack electric power are U_{ox}–T_{ox} and U_F–T_{ox}. The effect of the combination of U_{ox}–T_{ox} on the stack electric power is shown in Fig. 8.

We observe that the effects of the combination are important especially at high current values. In fact, the effects of the air utilization factor are emphasized due to the higher mass flows. Moreover, the effect of the air utilization factor is important if the air pre-heating temperature is low, while at high values of the air pre-heating temperature the effect of the air utilization factor is hardly reduced. In fact, the positive effect of a high air utilization factor on the stack equilibrium temperature is evident if the incoming air is slightly pre-heated, while if the incoming air has been already pre-heated at high temperature the effect of the air utilization factor on the stack temperature is reduced.

Finally, the effect of the combination of U_F–T_{ox} on the stack electric power is shown in Fig. 9.

Considering a combination of high values of U_F and T_{ox}, the reduction of the stack electric power due to a high fuel utilization factor could be compensated by a higher pre-heating

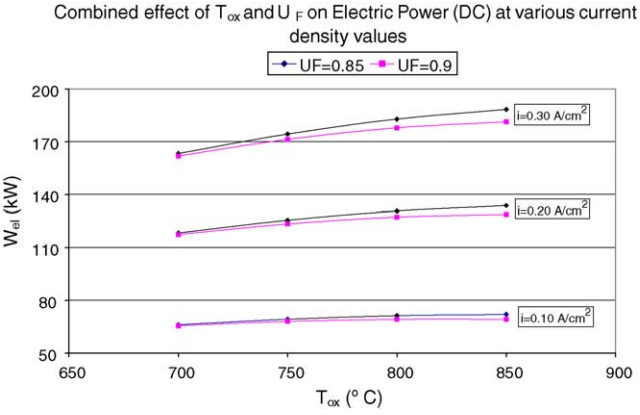

Fig. 9. Combined effect of the fuel utilization factor and the air pre-heating temperature on stack electric power.

of the incoming air. This effect is particularly emphasized at high current densities, where the curve slope is accentuated.

6.2. Recovered heat power

6.2.1. Considerations about main and interaction effects

The main and interaction effects on heat recovered are shown in Fig. 3 (low current density) and Fig. 4 (high current density).

Factors with no significant effects: An interesting notation is that the fuel preheating temperature has no effect on the recovered heat power; therefore, the fuel preheating could be avoided.
U_{ox} at high level: Positive main effect, due to increase of exhaust gas temperature and decrease of heat used for oxidant preheating.
U_F at high level: Negative main effect, due to decrease of heat recovered from the depleted fuel in the post-combustion chamber.
T_{ox} at high level: Negative main effect, due to better electric performances of the stack (and reduction of heat produced by irreversibility) and increase of oxidant preheating.
β at high level: Negative effect, an increase of β reduces the cell efficiency (and therefore increases the heat generated by irreversibility) but at the same time the fuel fraction at the post-combustor is reduced, and this is the prevailing factor explaining the negative effect; this negative effect is increased with a high fuel utilization factor (combination be).
Main and interaction effects at high cell current: At high cell current the main effects of the factors are emphasized.

6.2.2. Analysis of the effects of the significant factors

The effect of the air utilization factor is shown in Fig. 10.

With an increase of the air utilization factor, the heat recovered for cogeneration increases. This is due to several factors: higher stack equilibrium temperature, and consequently higher temperature of the stack exhaust flow; moreover, the heat flow used to preheat the oxidant is reduced because the inlet cathode mass flow is lower at lower air utilization factor. Even in this case, the effects are increased at high current densities, because the air mass flows are greater and this amplifies the effects of changing the air utilization factor.

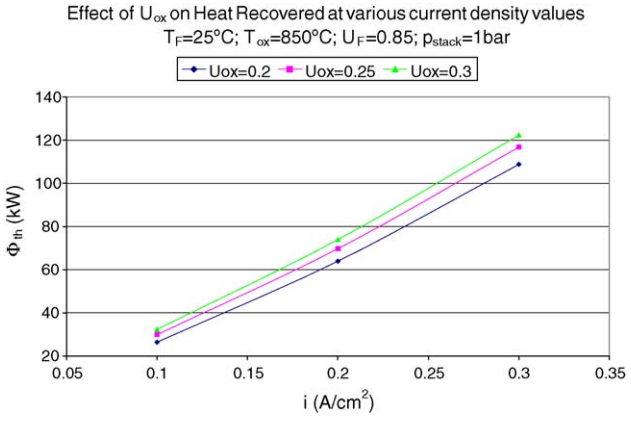

Fig. 10. Effect of the air utilization factor on heat recovered.

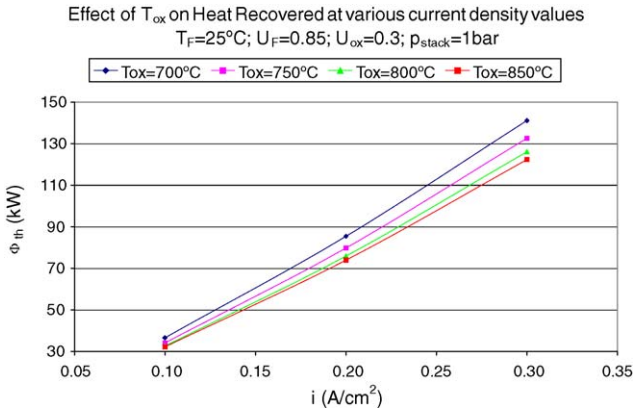

Fig. 11. Effect of the air pre-heating temperature on heat recovered.

A factor causing significant effects on the heat recovered is the air pre-heating temperature T_{ox}, as shown in Fig. 11.

The increase of the air pre-heating temperature has a negative effect on the heat recovered for cogeneration. This is due to the fact that the heat used to preheat the incoming air increases with the T_{ox} factor, and therefore the heat recovered for cogeneration is reduced. This happens even if the T_{ox} increase has a positive effect on the stack temperature and the exhaust temperature exiting the stack. As usual, the effects are emphasized at higher currents due to the higher mass flows.

The effect of the fuel utilization factor U_F on the heat recovered is shown in Fig. 12.

It is interesting to observe that the heat recovered for cogeneration increases at low fuel utilization factor values. In fact, with high U_F the fuel mass flow at the post-combustor is reduced, reducing the heat generated by post-combustion, and therefore the stack exhaust temperature is lower. To extract a higher heat flow from the stack exhaust is therefore better to operate with lower fuel utilization factor values.

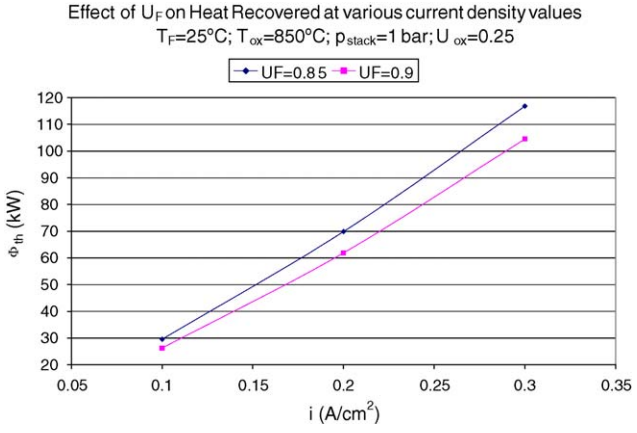

Fig. 12. Effect of the fuel utilization factor on heat recovered.

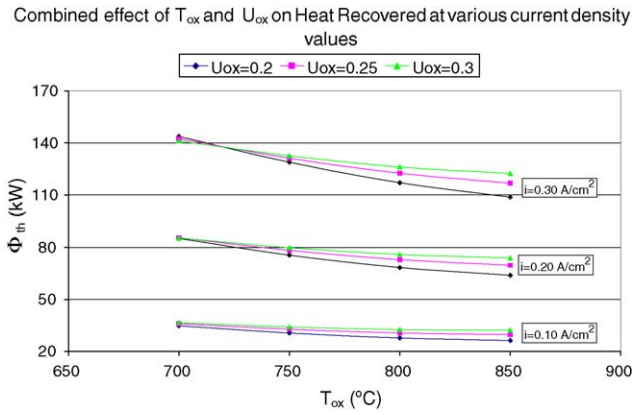

Fig. 13. Combined effect of the air utilization factor and the air pre-heating temperature on heat recovered.

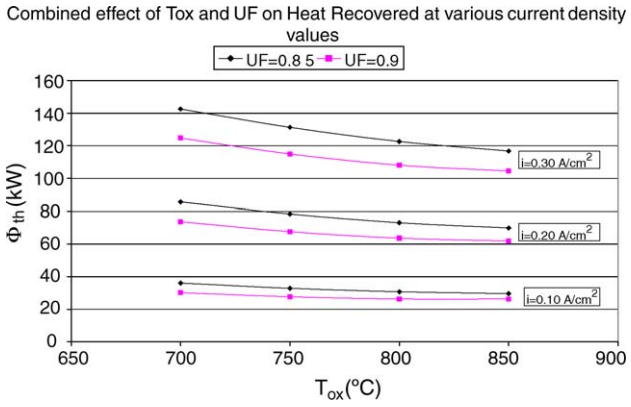

Fig. 14. Combined effect of the fuel utilization factor and the air pre-heating temperature on heat recovered.

This happens even if at high U_F the heat generated by irreversibility increases (as we noted, in this case the cell voltage is reduced), determining a higher stack equilibrium temperature, but this is not sufficient to assure an increase of the heat recoverable from the exhaust flow.

It is interesting to analyze the effects of some factor combinations. The factor combinations with a significant effect on the heat recovered for cogeneration are U_{ox}–T_{ox} and U_F–T_{ox}. The effect of the combination of U_{ox}–T_{ox} on the heat recovered is shown in Fig. 13.

We observe that the combination determines different effects at low or high current densities.

At fixed T_{ox}, a higher air utilization factor causes an increase of the stack equilibrium temperature, with a consequent increase of the cell voltage and reduction of the heat generated by irreversibility; at the same time, there is a reduced mass flow of incoming air which has to be preheated using the heat flow taken from the stack exhaust.

At low current densities, a high air utilization factor determines a higher value of stack electric power for every value of air pre-heating temperature. This could be due to the reason that in these operating conditions (low current, and therefore low stack irreversibility) the prevailing effect is the reduction of the incoming air, which has to be pre-heated, with a consequent increase of the heat recoverable for cogeneration.

At high current densities, the behavior is more complex. The operation irreversibility (and therefore the heat generated by the stack) is higher than at low current densities, and the role of the irreversibility generated heat is emphasized. Moreover, as we have observed in Fig. 12, the stack equilibrium temperature variation due to the variation of the air utilization factor is emphasized at low values of air pre-heating temperature. Therefore, if a low T_{ox} is fixed, at high currents is convenient to send to the stack a greater air mass flow (low air utilization factor) in order to exploit the higher irreversibility generated heat to obtain an increase of the heat recovered for cogeneration. Conversely, if a high T_{ox} is fixed, the behavior is the same observed at low current densities: in order to increase the heat recovered for cogeneration it is convenient to operate with a higher air utilization factor.

Finally, the effect of the combination of U_F–T_{ox} on the heat recovered is shown in Fig. 14.

Considering a combination of high values of U_F and T_{ox}, the effect is the reduction of the heat recovered for cogeneration. The negative effect is emphasized at high current densities.

7. Conclusions

In this paper, the computer experimental analysis, through a statistical methodology (ANOVA with Yate's method), of the single and combined effects of the main stack operation independent variables on the cogenerative (electricity and heat) performance of the EOS-CHP 100 SOFC Field Unit (Siemens) with methane feeding has been developed. The results can be summarized as follows:

- The fuel preheating temperature has no effect on both the electric power produced and the heat recovered; therefore, the fuel preheating could be avoided.
- The anode gas recycling fraction β shows no significant effects on the electric power, while it shows a negative effect on the heat recovered, because the fuel fraction at the post-combustor is reduced; therefore it could be fixed at the value indicated by the plant manuals.
- *U_{ox} at high level*: It shows positive main effect on the electric power, because of better performances in terms of internal thermal management and single cell electric efficiency, due to increase of cell temperature and decrease of cell overpotentials; at the same time, it shows positive main effect on the heat recovered, due to increase of exhaust gas temperature and decrease of heat used for oxidant preheating.
- *U_F at high level*: It shows negative main effect on the electric power, due to decrease of hydrogen partial pressure at cell anode and consequent decrease in Nernst voltage; at the same time, it shows a negative main effect on the heat

recovered, due to decrease of heat recovered from wasted fuel in post-combustion chamber.

- T_{ox} *at high level*: It shows positive main effect on the electric power, due to increase of cell temperature and decrease of cell overpotentials; at the same time, it shows a negative main effect on the heat recovered, due to better electric performances of the stack (and reduction of heat produced by irreversibility) and increase of oxidant preheating.
- At high cell current densities the main effects of the factors are emphasized because of the bigger mass flows inside the stack.

Acknowledgment

This work was financially supported by Gas Turbine Technologies (contract 470/2004), in the frame of the EOS project.

References

[1] E. Achenbach, Three-dimensional and time-dependent simulation of a planar solid oxide fuel cell stack, J. Power Sources 49 (1994) 333–348.
[2] N.F. Bessette II, W.J. Wepfer, J. Winnick, A mathematical model of a solid oxide fuel cell, J. Electrochem. Soc. 142 (1995) 3792–3800.
[3] A.F. Massardo, F. Lubelli, Internal reforming solid oxide fuel cell-gas turbine combined cycles (IRSOFC-GT). Part A. Cell model and cycle thermodynamic analysis, J. Eng. Gas Turbines Power 122 (2000) 27–35.
[4] A.F. Massardo, L. Magistri, Internal reforming solid oxide fuel cell–gas turbine combined cycles (IRSOFC-GT). Part B. Exergy and thermoeconomic analyses, J. Eng. Gas Turbines Power 125 (2003) 67–74.
[5] F. Marsano, L. Magistri, A.F. Massardo, Ejector performance influence on a solid oxide fuel cell anodic recirculation system, J. Power Sources 129 (2004) 216–228.
[6] S. Campanari, Thermodynamic model and parametric analysis of a tubular SOFC module, J. Power Sources 92 (2001) 26–34.
[7] E. Riensche, U. Stimming, G. Unverzagt, Optimization of a 200 kW SOFC cogeneration power plant. Part I. Variation of process parameters, J. Power Sources 73 (1998) 251–256.
[8] E. Riensche, J. Meusinger, U. Stimming, G. Unverzagt, Optimization of a 200 kW SOFC cogeneration power plant. Part II. Variation of the flowsheet, J. Power Sources 71 (1998) 306–314.
[9] A.D. Rao, G.S. Samuelsen, Analysis strategies for tubular solid oxide fuel cell based hybrid systems, J. Eng. Gas Turbines Power 124 (2002) 503–509.
[10] A.D. Rao, G.S. Samuelsen, A thermodynamic analysis of tubular solid oxide fuel cell based hybrid systems, J. Eng. Gas Turbines Power 125 (2003) 59–65.
[11] S. Primdahl, M. Mogensen, Oxidation of hydrogen on Ni/yttria-stabilized zirconia cermet anodes, J. Electrochem. Soc. 144 (1997) 3409–3419.
[12] L.G.J. De Hart, K. Mayer, U. Stimming, I.C. Vinke, Operation of anode-supported thin electrolyte film solid oxide fuel cells at 800 °C and below, J. Power Sources 71 (1996) 302–305.
[13] K. Sasaki, Y. Hori, R. Kikuchi, K. Eguchi, A. Ueno, Current–voltage characteristics and impedance analysis of solid oxide fuel cells for mixed H_2 and CO gases, J. Electrochem. Soc. 149 (2002) 227–233.
[14] A. Momma, Y. Kaga, K. Takano, K. Nozaki, A. Negishi, K. Kato, T. Inagaki, H. Yoshida, K. Hosoi, K. Hoshino, T. Akbay, J. Akikusa, M. Yamada, N. Chitose, AC impedance behaviour of practical size single cell SOFC under DC current, Solid State Ion. 174 (2004) 87–95.
[15] P. Holtappels, L.G. De Haart, U. Stimming, I.C. Vinke, M. Mogensen, Reaction of CO/CO_2 gas mixtures on Ni–YSZ cermet electrodes, J. Appl. Electrochem. 29 (1999) 561–568.
[16] A. Weber, B. Sauer, A. Muller, D. Herbstritt, E. Ivers-Tiffée, Oxidation of H_2, CO and methane in SOFCs with Ni/YSZ–cermet anodes, Solid State Ion. 152 (2002) 543–550.
[17] S. Gopalan, G. DiGiuseppe, Fuel sensitivity tests in tubular solid oxide fuel cells, J. Power Souces 125 (2004) 183–188.
[18] T. Iwata, Characterization of Ni–YSZ anode degradation for substrate-type solid oxide fuel cells, J. Electrochem. Soc. 143 (1996) 1521–1525.
[19] S. Primdahl, M. Mogensen, Durability and thermal cycling of Ni/YSZ cermet anodes for solid oxide fuel cells, J. Appl. Electrochem. 30 (2) (2000) 247–257.
[20] H. Sumi, K. Ukai, Y. Mizutani, H. Mori, C.J. Wen, H. Takahashi, O. Yamamoto, Performance of nickel–scandia-stabilized zirconia cermet anodes for SOFCs in 3% H_2O–CH_4, Solid State Ion. 74 (2004) 151–156.
[21] M.J. Jorgensen, P. Holtappels, C.C. Appel, Durability test of SOFC cathodes, J. Appl. Electrochem. 30 (2000) 411–418.
[22] R. Peters, R. Dahl, U. Kluttgen, C. Palm, D. Stolten, Internal reforming of methane in solid oxide fuel cell systems, J. Power Sources 106 (2002) 238–244.
[23] C.M. Finnerty, R.M. Ormerod, Internal reforming over nickel/zirconia anodes in SOFCs operating on methane: influence of anode formulation, pre-treatment and operating conditions, J. Power Sources 86 (2000) 390–394.
[24] A. Gunji, C. Wen, J. Otomo, T. Kobayashi, K. Ukai, Y. Mizutani, H. Takahashi, Carbon deposition behavior on Ni–ScSZ anodes for internal reforming solid oxide fuel cells, J. Power Sources 131 (2004) 285–288.
[25] C.M. Finnerty, N.J. Coe, R.H. Cunningham, R.M. Ormerod, Carbon formation on and deactivation of nickel-based/zirconia anodes in solid oxide fuel cells running on methane, Catal. Today 46 (1998) 137–145.
[26] R. Peters, E. Riensche, P. Cremer, Pre-reforming of natural gas in solid oxide fuel-cell systems, J. Power Sources 86 (2000) 432–441.
[27] J. Meusinger, E. Rienche, U. Stimming, Reforming of natural gas in solid oxide fuel cell systems, J. Power Sources 71 (1998) 315–320.
[28] K. Kendall, C.M. Finnerty, G. Saunders, J.T. Chung, Effects of dilution on methane entering an SOFC anode, J. Power Sources 106 (2002) 323–327.
[29] I. Drescher, W. Lehnert, J. Meusinger, Structural properties of SOFC anodes and reactivity, Electrochim. Acta 43 (1998) 3059–3068.
[30] F. Iguchi, Y. Endo, T. Ishida, T. Yokobon, H. Yugami, T. Otake, Y. Kawada, J. Mizusaki, Oxygen partial pressure dependence of creep on yttria-doped ceria ceramics, Solid State Ion. 176 (2005) 641–644.
[31] W. Li, K. Hasinka, M. Seabaugh, S. Swartz, J. Lannutti, Curvature in solid oxide fuel cells, J. Power Sources 138 (2004) 145–155.
[32] S. Campanari, P. Iora, Definition and sensitivity analysis of a finite volume SOFC model for a tubular cell geometry, J. Power Sources 132 (2004) 113–126.
[33] N. Autissier, D. Larrain, J.V. Herle, D. Favrat, CFD simulation tool for solid oxide fuel cells, J. Power Sources 131 (2004) 313–319.
[34] M. Lockett, M.J.H. Simmons, K. Kendall, CFD to predict temperature profile for scale up of micro-tubular SOFC stacks, J. Power Sources 131 (2004) 243–246.
[35] S.H. Chan, K.A. Khor, Z.T. Xia, A complete polarization model of a solid oxide fuel cell and its sensitivity to the change of cell component thickness, J. Power Sources 93 (2001) 130–140.
[36] S.H. Chan, K.A. Khor, X.J. Chen, Cathode micromodel of solid oxide fuel cell, J. Electrochem. Soc. 151 (2004) 164–172.
[37] P. Costamagna, A. Selimovic, M. Del Borghi, G. Agnew, Electrochemical model of the integrated planar solid oxide fuel cell (IP-SOFC), Chem. Eng. J. 102 (2004) 61–69.

[38] Y. Lu, L. Schaefer, P. Li, Numerical study of a flat-tube high power density solid oxide fuel cell. Part I. Heat/mass transfer and fluid flow, J. Power Sources 140 (2005) 331–339.
[39] A.M. Svensson, S. Sunde, K. Nisancioglu, A mathematical model of the porous SOFC cathode, Solid State Ion. 86–88 (1996) 1211–1216.
[40] A.V. Virkar, J. Chen, C.W. Tanner, J.W. Kim, The role of electrode microstructure on activation and concentration polarizations in solid oxide fuel cells, Solid State Ion. 131 (2000) 189–198.
[41] K. Huang, Gas-diffusion process in a tubular cathode substrate of an SOFC—theoretical analysis of gas-diffusion process under cylindrical coordinate system, J. Electrochem. Soc. 151 (2004) 716–719.
[42] M.A. Khaleel, Z. Lin, P. Singh, W. Surdoval, D. Collin, A finite element analysis modeling tool for solid oxide fuel cell development: coupled electrochemistry, thermal and flow analysis in MARC, J. Power Sources 130 (2004) 136–148.
[43] R.A. George, Status of tubular SOFC field unit demonstrations, J. Power Sources 186 (2000) 134–139.
[44] S.C. Singhal, Advances in solid oxide fuel cell technology, Solid State Ion. 135 (2000) 305–313.
[45] A. Weber, E.I. Tiffée, Materials and concepts for solid oxide fuel cells (SOFCs) in stationary and mobile applications, J. Power Sources 127 (2004) 273–283.
[46] M.C. Williams, J.P. Strakey, S.C. Singhal, U.S. distributed generation fuel cell program, J. Power Sources 131 (2004) 79–85.
[47] M.C. Williams, P. Joseph, Strakey, A. Wayne, Surdoval, The U.S. Department of Energy, Office of Fossil Energy Stationary Fuel Cell Program, J. Power Sources 143 (2005) 191–196.
[48] R.E. Walpole, R.H. Myers, Probability and Statistics for Engineers and Scientists, Prentice-Hall International Inc., New Jersey, 1993.
[49] M.F. Torchio, M. Santarelli, A. Nicali, Experimental analysis of the CHP performance of a PEMFC stack by a 24 factorial design, J. Power Sources, January, in press.